First Hit

Generate Collection Print

L1: Entry 2 of 3 File: DWPI Feb 28, 1989

DERWENT-ACC-NO: 1989-254832
DERWENT-WEEK: 198935


TITLE: Rain drops dimensions measurement - with acoustic signal modulated by rain-drops and modulated signals are recorded by counter according to lengths

INVENTOR: BAULIN, A D; BULKIN, V V ; ZAVGORODNE, S A

PATENT-ASSIGNEE:

| ASSIGNEE | CODE |
|---|---|
| MUROMSK VLAD POLY | VLAD |

PRIORITY-DATA: 1986SU-4086901 (April 14, 1986)

Search Selected Search ALL Clear

PATENT-FAMILY:

| PUB-NO | PUB-DATE | LANGUAGE | PAGES | MAIN-IPC |
|---|---|---|---|---|
| SU 1462182 A | February 28, 1989 | | 002 | |

APPLICATION-DATA:

| PUB-NO | APPL-DATE | APPL-NO | DESCRIPTOR |
|---|---|---|---|
| SU 1462182A | April 14, 1986 | 1986SU-4086901 | |

INT-CL (IPC): G01N 29/02; G01W 1/14

ABSTRACTED-PUB-NO: SU 1462182A
BASIC-ABSTRACT:

An acoustic field is formed in body (3) by an emitter connected to a generator and the acoustic field is registered by a detector, the signal from which passes through an amplifier, rectifier and length selector (7) to unit (9) of counters. Raindrops passing into body (3) modulate the amplitude of detected signals and selector (7) passes modulated signals to the corresponding counter according to lengths. Each counter records drops with dimensions in a determined range.

USE - Measuring dimensions of raindrops using ultrasonic vibrations. bul. 8/28.2.89

CHOSEN-DRAWING: Dwg.1/1

TITLE-TERMS: RAIN DROP DIMENSION MEASURE ACOUSTIC SIGNAL MODULATE RAIN DROP MODULATE SIGNAL RECORD COUNTER ACCORD LENGTH

СОЮЗ СОВЕТСКИХ СОЦИАЛИСТИЧЕСКИХ РЕСПУБЛИК

(19) SU (11) 1462182 A1

(51) 4 G 01 N 29/02, G 01 W 1/14

ГОСУДАРСТВЕННЫЙ КОМИТЕТ ПО ИЗОБРЕТЕНИЯМ И ОТКРЫТИЯМ ПРИ ГКНТ СССР

# ОПИСАНИЕ ИЗОБРЕТЕНИЯ

## К АВТОРСКОМУ СВИДЕТЕЛЬСТВУ

(21) 4086901/25-28
(22) 14.04.86
(46) 28.02.89. Бюл. № 8
(71) Муромский филиал Владимирского политехнического института
(72) В.В.Булкин, А.Д.Баулин, С.А.Завгороднев, Ю.В.Киселев и Е.Ю.Фирсов
(53) 620.179.16 (088.8)
(56) Авторское свидетельство СССР № 484451, кл. G 01 N 29/00, 1972.

Красненко Н.П. Акустическое зондирование атмосферы. - М.: Наука, 1986, с.50-72.

(54) СПОСОБ ИЗМЕРЕНИЯ РАЗМЕРА КАПЕЛЬ ОСАДКОВ

(57) Изобретение относится к контрольно-измерительной технике и может быть использовано для измерения разлива капель осадков с помощью ультразвуковых колебаний. Целью изобретения является повышение точности измерения. Способ измерения размера капель осадков осуществляется следующим образом. В исследуемой среде возбуждают упругие колебания. Принимают акустический сигнал, прошедший заданное расстояние в исследуемой среде. Измеряют амплитуду принятого сигнала. Поскольку при нахождении капли в зоне распространения упругих волн часть энергии отражается от частицы обратно, то и амплитуда принятого акустического сигнала будет уменьшаться, т.е. за время пребывания капли в точке акустических волн будет происходить модуляция принятого акустического сигнала. Чем больше частица, тем с большей скоростью она падает и тем меньше будет время модуляции амплитуды. Измеряют время модуляции амплитуды принятого акустического сигнала и по измеренному времени определяют размер капель осадков. 1 ил.

(19) SU (11) 1462182 A1

1

Изобретение относится к контрольно-измерительной технике и может быть использовано для измерения размера капель осадков с помощью ультразвуковых колебаний.

Целью изобретения является повышение точности измерения.

На чертеже представлено устройство для реализации способа измерения размера капель осадков.

Устройство содержит генератор 1, соединенный с акустическим излучателем 2, корпус 3, в котором помещены акустический излучатель 2 и акустический приемник 4. К выходу приемника 4 последовательно подключены усилитель 5, детектор 6 и селектор 7 длительности. В верхней части корпуса 3 имеется отверстие 8. Выходы селектора 7 длительности соединены с соответствующими входами блока 9 счетчиков.

2

Способ измерения размера капель осадков осуществляют следующим образом.

В корпусе 3 создается с помощью акустического излучателя 2 акустическое поле. Акустический излучатель 2 возбуждается от генератора 1 электрических сигналов. Создаваемое внутри корпуса 3 акустическое поле принимается акустическим приемником 4. Преобразованный сигнал затем поступает на усилитель 5, детектор 6 и селектор 7 длительности. При отсутствии частиц осадков в корпусе 3 сигнал, принимаемый акустическим приемником 4, не изменяется по амплитуде. Частицы осадков, попадающие в корпус 3 через отверстие 8, отражают часть акустической энергии, возбуждаемой акустическим излучателем 2. При этом уменьшается амплитуда акустического сигнала, принимаемого приемником 4. Это изменение амплитуды наблюдается в течение всего времени пребывания капли в корпусе 3 при ее падении, т.е. при прохождении частицы осадков через корпус 3 происходит модуляция амплитуды принимаемого акустического сигнала. Скорость падения капли однозначно связана с ее размерами. Это позволяет по измеренной скорости падения капли оценить ее размеры. При этом в зависимости от скорости изменяется время пребывания частицы в корпусе 3. Таким образом, информация о размерах капли получается не по параметрам принятого акустического сигнала, а по факту наличия модуляция этого сигнала в течени определенного времени, что дает возможность повысить точность измерений. Измеряется время, в течение которого изменяется амплитуда принятого акустического сигнала, т.е. происходит его модуляция. Для этого селектор 7 длительности осуществляет селекцию принятых импульсов, направляя их в зависимости от длительности на один из счетчиков блока 9 счетчиков. Количество счетчиков определяется необходимой степенью точности измерений. Каждый из счетчиков фиксирует наличие частицы с размерами, соответствующими определенному диапазону.

## Формула изобретения

Способ измерения размера капель осадков, основанный на направлении на осадки пучка акустических колебаний, приеме этих колебаний, измерении амплитуды принятого сигнала и определении размера капель осадков с учетом измеренной амплитуды, о т л и ч а ю щ и й с я тем, что, с целью повышения точности измерения, пропускают капли осадков через пучок акустических колебаний, измеряют время изменения принятого сигнала и определяют размер капель осадков по измеренному времени.

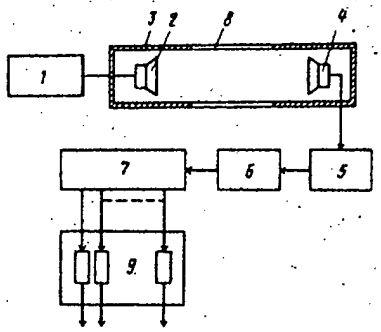


Составитель С.Волков
Редактор Н.Горват Техред М.Ходанич Корректор С. Патрушева
Заказ 667/41 Тираж 788 Подписное
ВНИИПИ Государственного комитета по изобретениям и открытиям при ГКНТ СССР
113035, Москва, Ж-35, Раушская наб., д. 4/5
Производственно-издательский комбинат "Патент", г. Ужгород, ул. Гагарина,101

# A Stochastic Raindrop Time Distribution Model

J. LAVERGNAT AND P. GOLÉ

*Centre d'Etude des Environnements Terrestre et Planétaires, Velizy, France*

(Manuscript received 25 February 1997, in final form 5 December 1997)

ABSTRACT

A disdrometer simultaneously measuring time of arrival and size of raindrops was set up in the Paris, France, area. Data collected over a period of 25 months (May 1992 to May 1994) are presented and analyzed to derive a long-term temporal model governed by a renewal process whose survival law is a Bi-Pareto law of the third kind. The model thus found allows nearly nine orders of magnitude of the time intervals between raindrops to be mathematically represented at the same time using only six parameters.

The analysis presented here does not consider rainfall intensity and the nature of rain (convective, stratiform, etc.) as classification parameters. This approach, which may at first sight seem objectionable, is justified by the quality of the statistical inferences that can be made from the model. Two such applications are described—namely, the prediction of the total fallen-water height and the conversion between various rain gauge integration times, which are often necessary for telecommunications purposes (for which only limited models are currently available). Since this kind of temporal data is rare, a comparison is also made with published data having the finest possible temporal resolution from the point of view of the fractal properties of rain, namely, its fractal dimension. A fairly good agreement was found with these other results and at the same time leads to a deeper insight into the fractal nature of rain.

This model provides a very satisfactory statistical representation of rain but does not intend to provide a physical interpretation of the observed temporal behavior of rain, which remains to be done.

## 1. Introduction

Rainfall is a very complex, naturally occurring phenomenon, many of the characteristics of which strongly influence in various ways a number of areas as different as hydrology (e.g., erosion and infiltration), meteorology, the earth's water cycle, remote sensing (e.g., observations from satellite platforms and radar observations), radio communications (e.g., rain attenuation), etc.

Rain is generally measured by means of rain gauges, which provide the total height of water fallen during a given time period, such as daily or hourly heights. Although this information is appropriate for climatologic or general meteorological purposes, its time resolution becomes insufficient when one tries to correlate rain with fast-changing phenomena, such as radar returns in rain or rain-induced attenuation of microwaves in telecommunications links. While rain gauges provide "flux" or intensity information—that is, an amount of water (height in millimeters) per time unit (hour)—another instrument, the disdrometer, measures the times of arrival and size of individual raindrops.

The idea that rain cannot be modeled appropriately by resorting only to the first group of parameters (fluxes), excluding the second one (sizes and times of arrival), can first be attributed to Smith (1993). There are many investigations of rain-gauge data, in which solutions are devised to overcome the problem of rain-gauge integration time (e.g., Waymire and Gupta 1981). For example, Olsson et al. (1993) devised a tipping-bucket rain gauge with a small bucket volume to obtain a resolution as fine as 0.035 mm $min^{-1}$.

Most studies devoted to rain use various classifier parameters (Laws and Parsons 1943; Hosking and Stow 1987). Some of these classifiers are related to the nature of rain, such as the notions of convective or stratiform precipitation. Others are related to precipitation intensity, rain rate being the most widely used. As an example, Feingold et al. (1986) classified raindrop size distributions according to rain rate.

This paper aims at analyzing the fine temporal structure of rain, rather than its intensity aspect, by using the data provided by a disdrometer that was part of a measurement campaign aimed at investigating the effects of the atmosphere on millimeter wave propagation (Gloaguen and Lavergnat 1995; Lavergnat et al. 1988). This device, in addition to providing 1-min size and velocity dual distributions—as was its first purpose—was improved so as to simultaneously record the size and time of arrival of raindrops falling through its collecting surface. The results presented below were ob-

*Corresponding author address:* Dr. Peter Golé, Centre d'Etudes des Environnments Terrestre et Planétaires, 10-12 avenue de l'Europe, 78140 Vélizy, France.

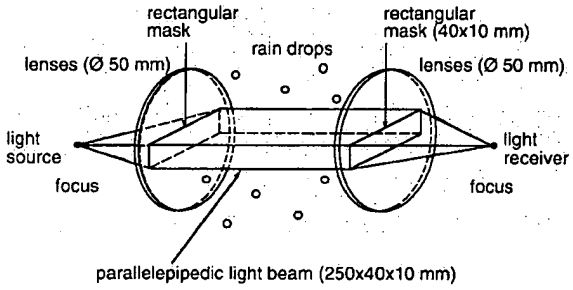


FIG. 1. Schematic layout and dimensions of the optical disdrometer.

tained during a total measurement period of nearly 2 yr for the distributions, and 4 months for the time-of-arrival data.

The approach used in this study was to model the long-term behavior of rain by analyzing the whole set of data without attempting to classify it according to event types or rain intensity or any other classifier. Other studies that take into account preclassifications are under way and will not be described here.

Nevertheless, other improvements seem to be indispensable and will be reviewed as a conclusion. The obtained results are encouraging and shed enough new light on rain structure that they were deemed useful to publish now.

After a brief description of the disdrometer used in the experiment, the obtained measurements are presented and a tentative interpretation is suggested in terms of a point process. Some interesting applications of the model are then derived. In the last section the same data are analyzed in terms of fractals and compared with already known results.

## 2. The experimental setup

The disdrometer used in the present experiment employs an infrared beam (Hauser 1984). An optical device transmits a parallel light beam (Fig. 1). On the receiving side, a photodiode delivers an electric signal that is proportional to the power of the received beam.

When a raindrop crosses the beam, it causes a change in the diode output voltage. Each drop generates a negative pulselike waveform, the magnitude and duration of which are related to the size and fall velocity of the drop, respectively. The device can distinguish two consecutive drops from each other if the falling edge of the pulse generated by the first one can be distinguished from the rising edge corresponding to the second one. For this to happen, the capture area has been designed to be sufficiently small (100 $cm^2$) to make coincidence of several drops in the beam negligible. Whenever coincidence occurs, this leads to unrealistic velocity–diameter combinations that are easily removed from the obtained data. The output of the photosensor was digitized and processed by a microcomputer. A calibration procedure consisting of moving a rod of a size corresponding to a 2-mm drop across the beam was automatically performed once a day in order to check a possible drift in the device's response. Two sets of data were recorded: one was aimed at assessing the fine temporal or short-term structure of rain and a second one, with a coarser resolution, was originally intended as auxiliary data to retrieve rain parameters influencing microwave propagation in the frame of the Olympus propagation program (Hughes 1993).

The first set of data was obtained by processing the digitized samples to provide the wanted parameters: time of arrival $t$ (resolution: 1 ms) and diameter $D$ (resolution: $10^{-3}$ mm, from 0 to 4.5 mm). In this dataset, fall velocities $V$ were available but were used only for the consistency check mentioned in the previous paragraph. They do not intervene in the development of the model. This first dataset covered a continuous time span of 4 months, from 22 October 1993 to 20 February 1994. A 1-week period has also been recorded from 19 to 26 July 1993 for a first assessment and is shown in Figs. 2a and 2b. Note that the beam thickness (1 cm) makes the time separation between raindrops unreliable for very small raindrops (<0.5 mm) since at a 1 m $s^{-1}$ fall velocity a raindrop resides only 10 ms in the beam. To overcome this problem, a new apparatus is under development, as the small size domain will be shown to be of importance here. The hardware section was developed by the Centre d'Etudes des Environnements Terrestre et Planétaires in Vélizy, France, while the acquisition software was developed by the Laboratoire de d'Etude des Transferts en Hydrologie et dans l'Environnement, in Grenoble, France.

Thus, a time series of triplets ($t$, $D$, $V$), characterizing each of the raindrops that have crossed the 100-$cm^2$ light beam, makes up the first or short-term dataset and will be used to measure interdrop time intervals with a 1-ms resolution. Though it may be objected that the time and space aspects of the measurement are mixed, the former can be considered as prevailing because of the small interception sectional area.

The data were then checked for consistency. Some peaks occur in the background noise of the measured signal, especially during nonrainy, fine weather periods. Due to their strong correlation with daily temperature variations, it was assumed that some of these spurious signals were caused by heat-induced turbulence or stray light. These peaks may be mistaken with pulses caused by actual raindrops, but on diameter–velocity (D–V) graphs they are easily detected as "false alarms," that is, drops with small diameters and very large velocities. To make sure these false alarms were removed, a threshold of 0.3 mm was applied to the obtained diameter data. It is shown in appendix A that this truncation has no impact on the model. This high time resolution dataset spanned a total time period of 14 months, with several interruptions ranging in length from 1 week to 3 months. The longest available continuous acquisition

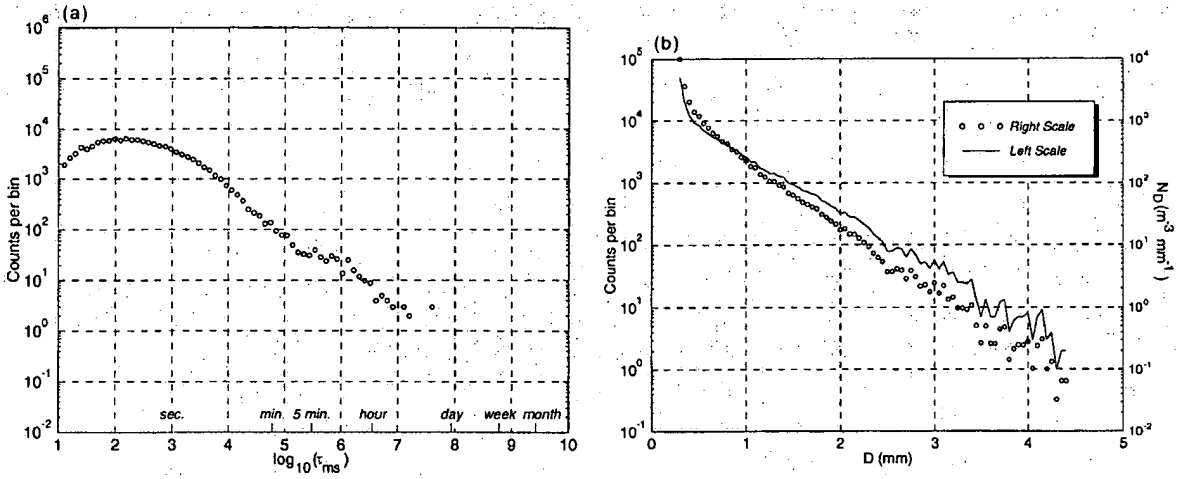


FIG. 2. (a) Distributions of interdrop time intervals and (b) sizes from 19 to 26 July 1993 (~1 week).

period was 4 months long and is the one used in the derivation of the model described here.

The second or long-term dataset was generated by software designed to give 1-min $D$–$V$ dual histograms, recorded as two-dimensional arrays, and was used to count the number of nonrainy time intervals with a 1-min resolution. It spanned a 2-yr period from May 1992 to May 1994 (25 months). To remove the influence of the above-mentioned spurious signals in the analysis of this second dataset, only those arrays with drop counts greater than 60 were kept for further analysis. This selection criterion resulted in a rejection percentage comparable to the 0.3-mm rejection threshold used for the first dataset. This procedure is justified by the fact that the time intervals that are looked for with this second dataset—namely, those greater than 10 min or so—correspond to the rain recovery time.

## 3. Observations

A first measurement campaign was carried out in Gometz-la-Ville, France, near Paris during a stormy period of 10 days (6–15 July 1993), which is not part of the first dataset mentioned above. Figure 2a shows a histogram (circles) of the decimal logarithm of time separations between raindrops, or interdrop intervals, designated $\tau$, as the random variable. This logarithmic random variable $\log_{10}(\tau)$ was counted in the range from 1 to 10 within bins of width 0.1. Note that the logarithm was used as the random variable due to the very wide range of orders of magnitude of the data (from 1 ms to more than 1 day). Another important point is that all of the interdrop time histograms presented here correspond to the specific measuring cross-sectional area of the disdrometer used in this study (100 cm$^2$), which therefore conditions the obtained histograms. This difficulty is inherent to any local device that is aimed at measuring rain and always has a finite size. Although it is beyond the scope of this paper to address this problem more deeply, simulations not presented here have shown that the size of the capture area mainly affects the shape of the $\log_{10}(\tau)$ histograms in the lower portion of their range (1–4), as longer time intervals correspond to time separations between individual rain events, which can be considered independent of the measuring cross section.

Figure 2b shows, as a solid line, the histogram, designated $n_D$, of drop diameters obtained during the same 10-day period, from 0 to 5 mm with bin widths of 0.5 mm. For comparison purposes with conventional drop size distributions (e.g., Marshall and Palmer 1948), Fig. 2b also shows as circles the corresponding number density of raindrops in m$^{-3}$ mm$^{-1}$, $N_D$, obtained from the histogram, $n_D$, through the following conversion:

$$N_D = \frac{n_D}{V(D)AT\Delta D},$$

where $V(D)$ is the terminal velocity of a drop of diameter $D$, $A$ is the cross-sectional area of the device, $T$ is the total time during which the distribution is measured, and $\Delta D$ is the histogram bin width. For $V(D)$, the fall velocity relation suggested by Atlas et al. (1977) has been used.

One is first surprised when looking at Fig. 2a that the distribution decreases rather steadily over more than seven decades, except for a stronger fluctuation and a slight change in slope after the 3–4-min histogram bin [$\log_{10}(\tau) = 3$–4] due to the relatively smaller number of data samples above this time range. The second surprise arises from the size histogram that, in addition to presenting a very high regularity, shows a steep increase in the region of small raindrops. This observed regularity must be attributed to the 1-week integration time used in this particular analysis and was not specific to these data.

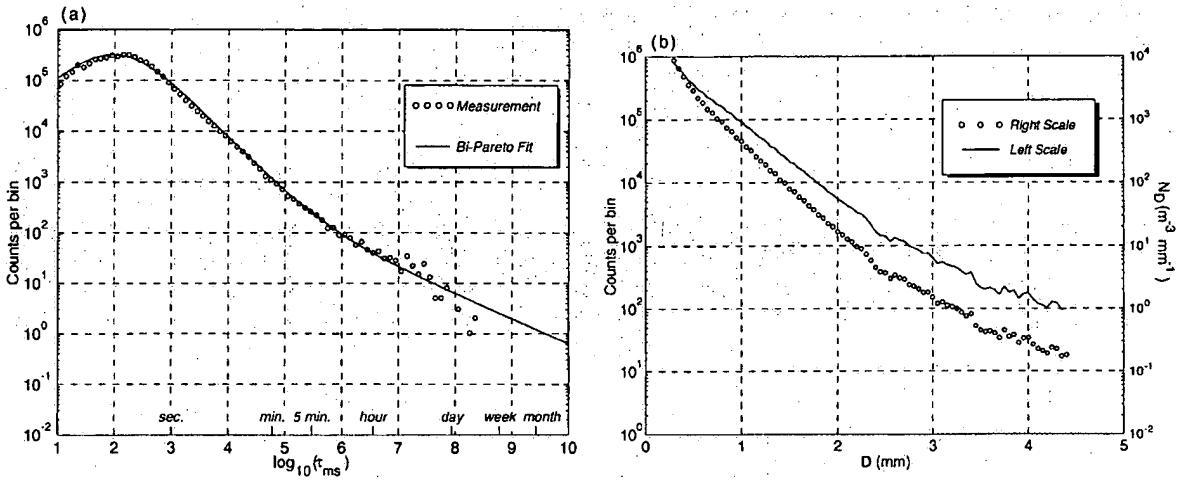


FIG. 3. (a) Distributions of interdrop time intervals and (b) sizes. High-resolution data from 22 October 1993 to 24 February 1994.

Figure 3a displays a histogram of the $\log_{10}(\tau)$ variable (circles) obtained (with the same range and bin width as Fig. 2) for the 4-month period of uninterrupted measurements provided by the first high-resolution dataset. It has a shape roughly similar to that shown in Fig. 2 [i.e., a maximum at $\log_{10}(\tau) = 2$, the same decreasing slope for $4 < \log_{10}(\tau) < 6$]. It also has an even greater regularity than that depicted in Fig. 2, and the largest nonrainy interval reaches a value of a little more than 2 days. In this histogram, the change in slope again clearly appears near the 5-min histogram bin.

Figure 3b shows, as a solid line, the drop size histogram obtained for the same 4-month high-resolution dataset. This figure also shows as circles, as in Fig. 2b, the size distribution of raindrops in $m^{-3}$ $mm^{-1}$, with a corresponding scale on the right of the graph. For simplicity, the models developed in the following sections were derived from the size histograms in counts per bin and not from the size distributions in $m^{-3}$ $mm^{-1}$. This distribution also has a more regular shape than the 1-week drop size data due to the increased number of samples. Although less pronounced than in the 1-week data, it still has an increasing slope near the lower limit of the analyzed diameter range (0.3–5 mm).

The possible causes of instrumental errors (e.g., spurious peaks in the recorded signal and splashing of drops) or software errors (for instance, counting two drops when there is only one, close to the background noise) that might have influenced the obtained drop size histogram shape were ruled out to explain the "abnormally" high proportion of small drops at the point where the apparatus reaches its sensitivity limits. The effect of spurious signals has been addressed by rejecting drops below 0.3 mm. The design of the disdrometer as a cylinder precludes any splashing of drops (Hauser et al. 1984). Multiple counting of drops leads to two consecutive drops in the measured time series having the same time stamp, so that both of these can be rejected, which has been performed.

## 4. Interpretation in terms of renewal processes

The histograms shown in Figs. 2 and 3 inherently suggest that the arrival of raindrops may be governed by a point renewal process. Their regularity and reproducibility strongly favor such a process. In addition, the correlation coefficient between two consecutive arrivals computed over the time period of Fig. 2 was found to be 0.08, a value that may be considered characteristic of renewal processes that are fundamentally not correlated.

Many authors (Waymire et al. 1981) who have investigated this subject had rejected the hypothesis that rain behaved according to a renewal process because this was difficult to combine with the clustering behavior also obvious in rain data. Complex processes—generally obtained by a combination of several simpler processes—were then suggested, such as Neyman–Scott or Davis (Waymire et al. 1981; Smith and Karr 1983).

Recently, Smith (1993) proposed a marked point process that involves a time-varying Poisson process "marked" by a lognormal drop size distribution. We shall also assume here that raindrop arrivals follow a renewal process and shall try to develop an empirical model to represent such a process. Moreover, the clustering behavior depends critically on the survival law of the process. Before going into details, the employed methodology will be reviewed briefly.

It should be pointed out that a renewal process may be determined either through the counting properties or the survival law. The former are simpler to obtain experimentally, but it is generally difficult to derive the underlying survival law. In the present experiment, we had the possibility of having many observations of the

survival law. This is why we chose to determine this law first.

When trying to determine the form of the renewal process in question, it may seem that a goodness-of-fit criterion would not be sufficient to correctly validate the model that is sought; however, it is a good indicator and should be understood as a first step in the model determination. The applications described in later sections were developed in part to check the validity of some of the consequences of the model derived in the following section. Furthermore, although this anticipates some of the results described below, the fact that this model allows the temporal distribution and drop size spectra to be intimately related to each other seems to be a very good indication of the interest of such a model.

*a. The renewal process*

As a first step, it will be assumed that the process is simple and that the first arrival time in the modeled time series is 0. If $\tau_i = t_{i+1} - t_i$ is the time interval separating two consecutive raindrops, or interdrop interval, the assumption of a renewal process states that the $\tau_i$'s are all independent and identically distributed. Their common distribution law, also known as a survival law, is either characterized by a cumulative distribution function $F(\tau)$ such that

$$F(\tau) = \text{Prob}\{\tau_i \leq \tau\}$$

or by a probability density function if it exists:

$$f(\tau) = \frac{dF(\tau)}{d\tau}.$$

Noting that a renewal process with an exponential survival law is a Poisson process, the histograms found from the measured data described in the previous section show that the process we are looking for is not Poisson distributed, as its slope is not exponential for large $\tau$'s, but one that varies, as a first approximation, as a decreasing power of $\tau$.

Among known probability density functions, Pareto's group exhibits a power behavior for large $\tau$'s and is therefore a good candidate. A closer look at the data in Figs. 2 and 3 shows that the histograms indeed fall off along a straight line after having reached their peak around the 2.5-ms abscissa and that the change in slope, which may be observed around the 5-min abscissa, seems to indicate that a more refined distribution function is needed. We thus attempted to derive a more elaborate model, though one still based upon the Pareto distribution.

As suggested in the previous section, the obtained histograms simultaneously represent widely different timescales. The approach chosen to refine the initially selected Pareto function, suggested by the first short-term analyses presented in the observations section, was to consider that the total distribution was an addition of two separate component Pareto laws, called a "Bi-Pareto law," and expressed by its probability density function as follows:

$$f(\tau) = p\frac{\alpha a^\alpha}{(\tau + a)^{\alpha+1}} + q\frac{\beta b^\beta}{(\tau + b)^{\beta+1}}, \qquad (1)$$

where $p$ and $q$ are normalization constants for the summation of both Pareto component functions to integrate to unity and are such that $p + q = 1$, so that (1) actually depends on five parameters ($a$, $b$, $\alpha$, $\beta$, and either $p$ or $q$).

Note that to perform a fit to the histograms of the random variable $\log_{10}(\tau)$ and not $\tau$ itself, as shown in Figs. 2 and 3, the $\tau$ distribution must first be multiplied by $\tau$. Also note that the fit criterion used throughout this study was to perform a least squares fit—that is, minimize the standard deviation between the logarithms of the measured and "theoretical" distributions.

The standard deviation was found to be 0.131 for this Bi-Pareto model. The first of the two components of the model represents the shorter time intervals and what happens within a rainy episode. As mentioned earlier, this component will be strongly dependent, through its $a$ and $\alpha$ parameters, on the size of the measuring cross section of the instrument. The second component, which accounts for the larger time intervals, expresses the spacing between rainy episodes and will not depend on the instrument size.

The least squares fit of this function to the histogram of Fig. 3a after applying a normalization constant $C$ [since, for simplicity, it was chosen to express histograms as "number of events per bin," that is, the number of $\log_{10}(\tau)$ samples found between two consecutive thresholds] gives the curve plotted as a solid line, with the following model parameters for $\tau$ in milliseconds:

$$\left\{\begin{array}{lll} a = 133, & b = 1220, & q = 1.12 \times 10^{-2}, \\ \alpha = 1.35, & \beta = 0.68, & p = 1 - q, \\ C = 1.235 \times 10^{-6} & & \end{array}\right\}. \qquad (2)$$

From the point of view of goodness of fit to experimental data, this model may be considered excellent. However, other mathematical expressions could as well be used instead of (1) with a similar quality of fit. Simplicity and the possibility to separate short-term from long-term events have decided in favor of model (1). However, this model nevertheless raises serious problems. The mean value of the interdrop time interval, provided it exists, is given by

$$\mu = \langle\tau\rangle = p\int_0^\infty \frac{\alpha a^\alpha \tau}{(\tau + a)^{\alpha+1}}\,d\tau + q\int_0^\infty \frac{\beta b^\beta \tau}{(\tau + b)^{\beta+1}}\,d\tau. \qquad (3)$$

It exists only if $\alpha$ or $\beta$ are both greater than unity. However, here, while $\alpha$ is greater than 1, this is not the

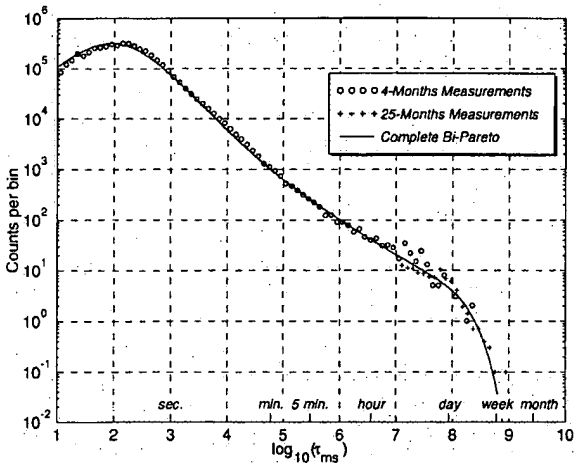


FIG. 4. Distributions of interdrop time intervals obtained from 4 months of data (O) and from 25 months of data (+).

case for $\beta$. Therefore, applying the model would imply that

- the process is not stationary and that
- the process has an "end," meaning that the average number of drops $N$ over an interval $[t, t + \delta]$ asymptotically decreases as follows:

$$\left.\begin{array}{r} E[N(t, t+\delta)] \to 0 \\ \text{for } t \to \infty \end{array}\right\} \forall\, \delta > 0,$$

which amounts to predicting an endless and overwhelming drought at some time in the future (Feller 1957; Karlin and Taylor 1975). Obviously, none of these consequences are physically acceptable. To remove these inconsistencies, it is necessary to admit that the probability density function $f(\tau)$ of (1) becomes invalid for very large $\tau$'s.

To investigate this point, the low-resolution dataset, which covered a full noninterrupted 25-month period, was used. Although this dataset has a lower time resolution, the very large time period it covers allows longer interdrop time intervals to be studied. It leads to a histogram of its own, which gives an indication of how the tail of the overall distribution should look. We chose to display it on the same graph as that obtained from the high time resolution dataset. To combine the short- and long-term histograms, the latter was normalized in such a way that it appears as a continuation of the former at the tail of the high-resolution dataset since what we are looking for is essentially the behavior of the histogram at longer interdrop time intervals; that is, we are checking that the histogram actually falls down for large $\tau$'s. The result is shown in Fig. 4, in which the circles and crosses identify the short- and long-term data, respectively. This pseudonormalization procedure leads to counts less than unity in the second histogram for abscissa greater than about 3 days. What is important to note in this figure is an abrupt decrease in the histogram, somewhere around a 1-day interdrop interval. The experimental combined histograms thus obtained suggest that an exponential decrease occurs for the larger interdrop time intervals.

To take this exponential decrease into account in the model, it is, however, not possible to directly multiply the Bi-Pareto distribution function $f(\tau)$ by an exponentially decreasing factor of the form $e^{-\lambda_0\tau}$, as it would not integrate to unity. This problem can be overcome when noting that

$$\int_0^\infty e^{-\lambda_0\tau} f(\tau)\, d\tau = 1 - \int_0^\infty \lambda_0 F_c(\tau) e^{-\lambda_0\tau}\, d\tau,$$

where $F_c(\tau)$ is the complementary cumulative distribution function defined as $F_c(\tau) = 1 - \int_0^\tau f(x)\, dx$. From this, it may be seen that to have a statistical distribution whose main form is $f(\tau)$ and that shows an exponential decrease for large $\tau$'s, the Bi-Pareto distribution $f(\tau)$ has to be transformed as follows:

$$\varphi(\tau) = e^{-\lambda_0\tau}[f(\tau) + \lambda_0 F_c(\tau)]. \tag{4}$$

For sufficiently small values of $\lambda_0$ and for small $\tau$'s, $\varphi(\tau) \approx f(\tau)$, while for large $\tau$'s, $\varphi(\tau) = e^{-\lambda_0\tau} f(\tau)$, which shows that the function has the desired exponential decrease. When applied to the Bi-Pareto law (1), the transformation suggested in (4) leads to the following probability density function:

$$f(\tau) = e^{-\lambda_0\tau}\left[p\frac{a^\alpha[\alpha + \lambda_0(\tau + a)]}{(\tau + a)^{\alpha+1}} + q\frac{b^\beta[\beta + \lambda_0(\tau + b)]}{(\tau + b)^{\beta+1}}\right], \tag{5}$$

which will be called the Complete Bi-Pareto model, and to the associated cumulative distribution function

$$F(\tau) = 1 - e^{-\lambda_0\tau}\left[p\frac{a^\alpha}{(\tau + a)^\alpha} + q\frac{b^\beta}{(\tau + b)^\beta}\right]. \tag{6}$$

Keeping the values of the parameters already obtained above, the value of $\lambda_0$ can be derived through a best fit to the experimental histogram of Fig. 4, again using a least squares fit between the logarithms of the model in (5) (after multiplying it by $\tau$, as mentioned above) and the experimental histogram. The value found was $\lambda_0 = 10^{-8}$. The theoretical curve thus obtained is plotted as a solid line in Fig. 4, where it may be seen that the probability density function (5) (after multiplication by an appropriate normalization constant) is in very good agreement with the data collected during 25 months.

This distribution, as expected, provides a finite average interdrop time interval. Since $a\lambda_0$ and $b\lambda_0$ are small, the average interdrop interval $\mu$ (3) may be given a simple asymptotic expression

$$\mu = \langle\tau\rangle \approx p\frac{a}{\alpha - 1} + qb^\beta\lambda_0^{\beta-1}\Gamma(1 - \beta), \tag{7}$$

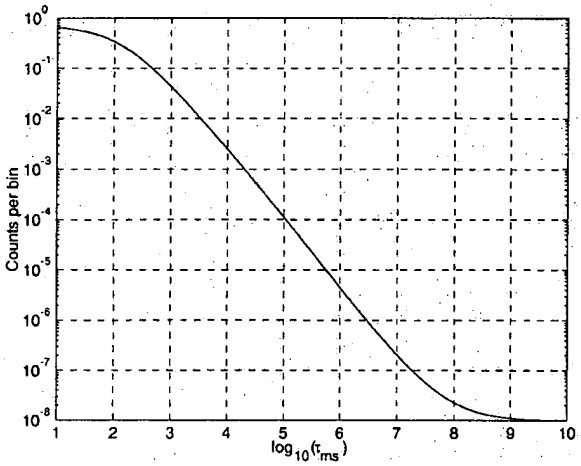


FIG. 5. Occurrence rate function $s(\tau)$.

which leads to the numerical result that $\mu = 0.38 + 1.4 = 1.78$ s for our experimental setup and observation period. The value of the occurrence rate, also known as the hazard function, $s(\tau) = f(\tau)/[1 - F(\tau)]$, which indicates the probability that a raindrop arrives between time points $\tau$ and $\tau + d\tau$, provided none has arrived before time $\tau$, is shown in Fig. 5. For small $\tau$'s, $s(\tau)$ is constant. From 0.1 s to 1 day it decreases as $1/\tau$, which may be interpreted by saying that the more one has been waiting, the more one will be waiting. In other words, the more the rain rate decreases, the more it is likely to end. This is a common sense observation that leads to the subjective feeling of clustering. Fortunately enough, this trend does not last, as $s(\tau)$ asymptotically goes to $\lambda_0$, which is a physical expression of the revisited proverb: "After sunshine comes the rain!"

### b. *Relationship between size and time of arrival distributions*

The question of how the survival law defined in (5) is generated will now be addressed. One of the remarkable properties of Pareto distributions is that they can be obtained by a combination of an exponential distribution and a gamma distribution (Harris 1968). Assuming these two distributions write

$$p(\tau) = \lambda e^{-\lambda\tau} \tag{8}$$

and

$$\rho(\lambda;\, \alpha,\, a,\, \lambda_0) = \begin{cases} \dfrac{a^\alpha}{\Gamma(\alpha)}(\lambda - \lambda_0)^{\alpha-1}e^{-a(\lambda-\lambda_0)}, & \lambda \geq \lambda_0, \\ 0 & \lambda < \lambda_0, \end{cases} \tag{9}$$

their mixture leads to the Complete Bi-Pareto's distribution, namely, one has

$$\int_0^\infty \Pi(\lambda)p(\tau)\, d\lambda = e^{-\lambda_0\tau}\left[p\frac{a^\alpha[\alpha + \lambda_0(\tau + a)]}{(\tau + a)^{\alpha+1}} + q\frac{b^\beta[\beta + \lambda_0(\tau + b)]}{(\tau + b)^{\beta+1}}\right], \tag{10}$$

which is the expression of the Complete Bi-Pareto model of (5). In this expression, $\Pi(\lambda)$ is a combination of two "shifted" gamma distributions as defined in (9):

$$\Pi(\lambda) = p\rho(\lambda;\, \alpha,\, a,\, \lambda_0) + q\rho(\lambda;\, \beta,\, b,\, \lambda_0). \tag{11}$$

This raises the question of what such a distribution might physically correspond to. First looking at distribution (8), $\lambda$ represents the inverse mean time between two raindrops or the mean number of drops per time unit. Over a time period $T$, $\lambda T$ then asymptotically represents the number of drops with "parameter" $\lambda$. Since the drop size is the main characterizing parameter, it is therefore tempting to link $\lambda$ with the effective drop diameter $D$, the involved relation obviously being monotonous.

This assumption can be tested using many different distributions that relate $\lambda$ with $D$. It is desirable to prevent the drop size distribution model from overestimating very small raindrops, which are the most numerous, as this might strongly bias physical quantities derived from the model, while avoiding singular points. After several tests, the following $\lambda$–$D$ relation was adopted and will be justified below:

$$\Lambda = \lambda - \lambda_0 = K(D - D_1)^\nu[1 - e^{-k(D-D_1)^\nu}]. \tag{12}$$

The following drop size probability density function is then obtained:

$$\Pi(D) = \Pi(\lambda)\left|\frac{d\lambda}{dD}\right| = \left[p\frac{a^\alpha}{\Gamma(\alpha)}\Lambda^{\alpha-1}e^{-a\Lambda} + q\frac{b^\beta}{\Gamma(\beta)}\Lambda^{\beta-1}e^{-b\Lambda}\right] \times \left[\frac{\nu\Lambda}{D} + \nu kD^{\nu-1}(KD^\nu - \Lambda)\right]. \tag{13}$$

Since (13) is a probability density function, it can be compared with the experimental histogram (Fig. 3b) only after having been normalized to the total number of drops. For experimental reasons, drops with diameters under 0.3 mm were rejected from the dataset as dubious, so that parameter $D_1$ in relation (13) is, of course, impossible to determine through a direct fitting process to the available data.

When $D_1$ is set to different values below 0.3 mm, the parameters indicated in Table 1 are found for the drop size distribution model. The influence of the model on such a physical quantity as the mean drop volume is indicated in the $\langle v \rangle$ column of Table 1.

TABLE 1. Best-fit parameters in relation (13) ($C$ is the normalization constant found in the fitting process).

| $D_1$ (mm) | $\upsilon$ | $K$ | $k$ | $\sigma$ | $\langle v \rangle$ (mm³) | $C$ |
|---|---|---|---|---|---|---|
| 0.05 | 0.55 | $3.5 \times 10^{-2}$ | 1.66 | 0.062 | 0.14 | $4.05 \times 10^5$ |
| 0.1 | 0.56 | $3.4 \times 10^{-2}$ | 1.70 | 0.061 | 0.18 | $3.65 \times 10^5$ |
| 0.2 | 0.57 | $3.3 \times 10^{-2}$ | 1.70 | 0.060 | 0.25 | $3.04 \times 10^5$ |

The obtained fitting results are all very good (standard deviations $\sigma$ close to 0.06 count units), as shown in Fig. 6, so that this criterion alone cannot be reliably resorted to here. This result is rather interesting for two reasons.

1) The final model that has been arrived at provides a coherent view of the survival and drop size distributions. Nevertheless, this does not mean that a "reason" why these distributions have the shape they have has been found. However, the fact that the model implies a coupling between drop sizes and arrival times opens new perspectives.

2) The value found for $\upsilon$ is the most surprising result. When referring to the work of Atlas and Ulrich (1977), who suggest the relation between the fall velocity at ground level and diameter

$$V(D) = 3.78D^{0.67}, \tag{14}$$

where $D$ is expressed in millimeters, it may be noted that parameter $\nu$ that has been found and is indicated in Table 1 differs only by 15% from the value of 0.67 shown in (14). The large value of $k$ leads to the result that whenever $D$ is greater than 0.5 mm, (12) can be approximated by $K(D - D_1)^\nu$ and is thus found to be very close to relation (14). The effect of the $1 - e^{-k(D-D_1)^\nu}$ term is that $\Pi(D)$ approaches 0 when $D$ approaches $D_1$, which is satisfactory. Here again we can regret only the lack of reliable data for small raindrops. Therefore, everything tends to show that the quantity $\Lambda$ in formula (12) is actually proportional to the ground-level fall velocity of raindrops.

### c. *Applications of the proposed model*

Rainfall rate is universally employed to characterize rain. It would therefore be interesting to investigate what the present model would be able to reveal in this respect. This question does not find a straightforward answer, as it is related to the counting aspect of the process, which hardly lends itself to analytical computations, at least in the case of survival law (5). However, classical calculations (appendix B) lead to a dual Laplace transform of the probability that a precipitated water height $h$ be exceeded over a given $[0, t]$ time interval

$$Q_c(u, s) = \frac{1 - f(s)}{\mu s^2 u} \frac{1 - p(u)}{1 - p(u)f(s)}, \tag{15}$$

where $p(u)$ is given by (B9) and $\mu$ is the average interdrop time given by (7). Expression (15) allows the two following problems to be tackled easily. They are selected not only to check the model's validity but also to show some of its practical applications.

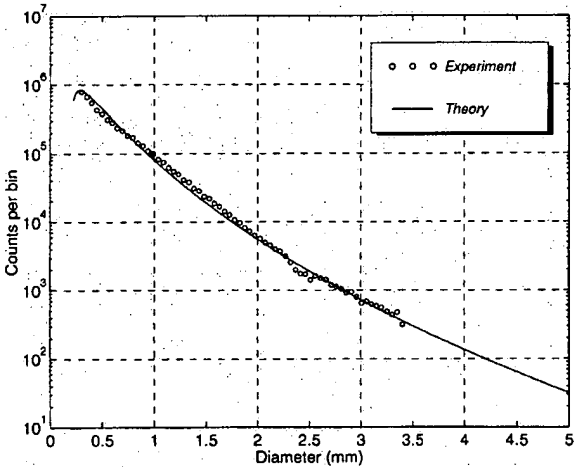


FIG. 6. Experimental (October 1993 to February 1994) and theoretical drop size distributions.

#### 1) AVERAGE PRECIPITATED WATER HEIGHT

The average precipitated water height can be obtained either directly from the basic renewal theorem applied to a cumulative process (Feller 1957) or through the relationship $\lim_{u \to 0} Q_c(u, t) = \int_0^\infty Q_c(h, t)\, dh$, which leads to

$$\langle H(t) \rangle = \frac{\langle v \rangle}{A\mu} t, \tag{16}$$

where $\langle v \rangle$ is the average raindrop volume and $A$ is the collecting area of the instrument. When using the value of $\mu$ reported above—that is, $\mu = 1.785$ s—and size distribution (13), which leads to $\langle v \rangle = 0.26$ mm³, the average yearly precipitated water height is

$$\langle H(t) \rangle_{\text{year}} = 549 \text{ mm}.$$

This value is in good agreement with that measured by means of a standard rain gauge located on the same site as the disdrometer, which led to a total rain height of 563 mm for the period from May 1992 to April 1993. However, this agreement should be regarded with caution, as the variability of cumulative rain height from one year to the next may exceed 100 mm.

Can this model explain such a variability? Appendix C gives a computation of the main elements that are needed to estimate the standard deviation of rain height that should be expected. Numerically, it is found to be $\sigma_H/\langle H \rangle = 3\%$. Such a small value is indicative of the fact that the model requires further refinement to account for seasonal or climatic variability. This point will be addressed in a further paper when sufficient data are available.

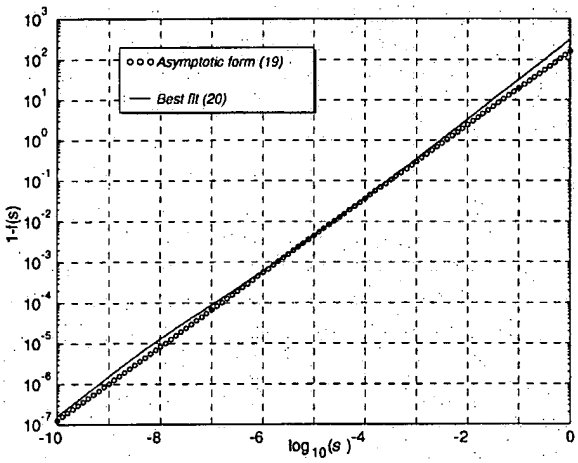


FIG. 7. Comparison between asymptotic and best-fit forms of the Laplace transform $f(s)$ of $f(\tau)$, as defined by (19) and (20), respectively.

### 2) CONVERSION BETWEEN RAIN RATES OBTAINED WITH VARIOUS INTEGRATION TIME

Designers of radio systems use predictions based on rainfall statistics derived from rain gauges with 1-min integration times (ITU-R 1990). However, the integration times of rain gauges may differ from one place to another and may reach 10 min or even an hour. In such cases, it is useful to derive statistics that would have been obtained for 1-min integration times from those available at other integration times. Traditionally (Segal 1986), one uses a conversion factor that depends on the considered exceedance probability and on the rain-gauge integration time.

The present model allows this problem to be addressed in a different way. When focusing on higher rain rates, the asymptotic value of $p(u)$ for $u \to 0$ may be used in $Q_c(u, s)$; that is, $p(u) = 1 - (\langle v \rangle / A)u = 1 - Bu$. This leads to (cf. appendix B)

$$Q_c(u, s) \approx \frac{1 - f(s)}{\mu s^2 f(s)} \times \frac{1}{u + \dfrac{1 - f(s)}{Bf(s)}}, \quad (17)$$

with the following inverse Laplace transform in $u$:

$$Q_c(h, s) \approx \frac{1 - f(s)}{\mu s^2 f(s)} e^{-h\{[1 - f(s)]/[Bf(s)]\}}. \quad (18)$$

For integration times greater than 1 min, the inverse transform in (18) will be influenced only by values of $s$ that are greater than $10^{-4}$. Thus, the asymptotic form of $f(s)$ may be used:

$$f(s) \approx 1 - p\frac{as}{\alpha - 1} - qb^{\beta}s(s + \lambda_0)^{\beta - 1}\Gamma(1 - \beta). \quad (19)$$

Figure 7 shows that this function may be approximated, for $s$ ranging from $10^{-8}$ to $10^{-3}$, by a function of the following kind:

$$f(s) \approx 1 - ds^{\xi}, \quad (20)$$

where $\xi = 0.92$ and $d = 10^{2.33}$. Substituting (20) into (18), the following equation is obtained:

$$Q_c(h, s) = \frac{d}{\mu} s^{\xi - 2} e^{-(d/B)s^{\xi}h}. \quad (21)$$

Applying the scaling property of the Laplace transform leads to

$$Q_c(h, kt) \overset{\text{LT}}{\to} \frac{1}{k} Q_c\left(h, \frac{s}{k}\right),$$

from which it is derived that

$$Q_c\left(\frac{h}{k^{\xi}}, t\right) = k^{\xi - 1} Q_c(h, kt),$$

or using rain rate $r$ measured over interval $[0, t]$, with $r = h/t$,

$$Q_c(r, t) = k^{\xi - 1} Q_c(rk^{\xi - 1}, kt), \quad (22)$$

where $Q_c(r, t)$ is nothing but the cumulative probability function of rain rate $r$ that would be obtained with a rain gauge having an integration time $t$. Formula (22) thus allows a rain-rate distribution observed using an integration time $kt$ to be changed into one that would have prevailed for an integration time $t$.

To show how this model can be applied, data obtained using the same disdrometer, during a 1-yr period not overlapping the one used to develop the interdrop time distribution model (5), were analyzed using 1- and 10-min integration times.

The ITU-R model mentioned above has been derived from measured cumulative distributions, for the 5- and 10-min to 1-min conversions, and cannot be extended to other integration times. It has been obtained by fitting the ratio of the 5-min to the 1-min cumulative distributions measured in Canada, without considering the fine structure of the rain's temporal distribution.

This temporal information is contained in the present Complete Bi-Pareto model, which has led to the integration time conversion model suggested in (22). To check the validity of the present model and compare it to the ITU one, it is interesting to apply it to the common 10-min to 1-min conversion problem.

Under these conditions, factor $k$ in (22) is equal to 10, and $k^{\xi - 1}$ is equal to 0.768, assuming $\xi = 0.885$, as suggested in the previous section. From this, if $P_1$ is the probability that a rain rate $r_1$, measured with a 1-min integration time, is exceeded, then the probability $P_{10}$ that a rain rate $r_{10}$, measured with a 10-min integration time, is exceeded, would be given by

$$P_{10}(r_{10}) = P_1(r_1)/0.768$$

and

$$r_{10} = r_1 \times 0.768.$$

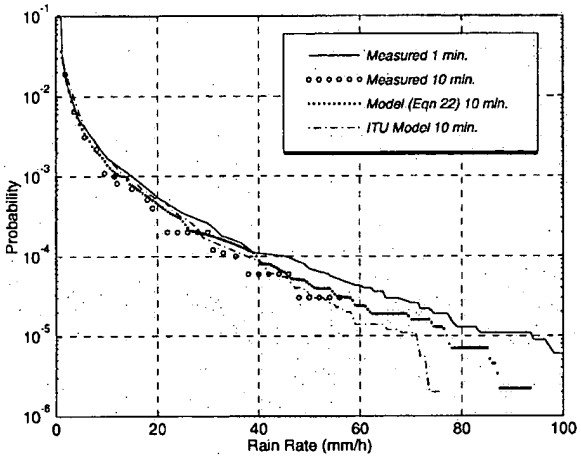


FIG. 8. Comparison between measured cumulative distributions of rain rate with 1- and 10-min integration times, given by the present model [(22)] and the ITU-R model.

In the ITU-R model, the corresponding relation is as follows:

$$P_{10}(r_{10}) = P_1(r_1)$$

and

$$r_{10} = \frac{r_1 \times 0.836}{[P_1(r_1) \times 100]^{0.0736}}.$$

The 0.836 factor in the above expression was defined as corresponding to climatic zone *E*, the site where our measurements were performed.

Figure 8 shows the cumulative distribution of rain rate using integration times of 1 min (continuous line) and 10-min (circles). The distribution obtained according to the present model [Eq. (22)] is plotted (dash–dot curve), and a comparison is provided with the ITU-R model (dots). Not only does this figure show a very good agreement between our model and observations but the present result is also in good agreement, at least up the 50 mm $h^{-1}$ level, with the ITU-R model obtained using a quite different and purely empirical approach and based on a very different data corpus.

The advantage of this model is that it is universal, in the sense that any combination of integration times can be used—contrary to the ITU one—that imposes 5-, 10-, and 15-min integration times.

## 5. A fractal point of view

Atmospheric phenomena, like many natural phenomena, have self-similarity properties in that their form does not change whatever the scale at which they are observed. Lovejoy and Mandelbrot (1985) presented a rain model with only one fractal dimension (which is the parameter relating the statistical properties to all observation scales). However, this approach does not allow all observations to be represented. Moreover, the fractal dimension seems to depend on the observation techniques used (e.g., rain gauge, radar, etc.). In a recent paper, Olsson et al. (1993) analyzed the similarity properties of a time series of data from a very high resolution rain gauge (0.035 mm $min^{-1}$). It is interesting to look at what our data and model may lead to using the same approach. The box-counting method developed by these authors was chosen due to its greater simplicity than the other suggested analysis methods.

The total observation time $T$ is divided into $n$ contiguous intervals of length $L$. Thus, $T = nL$. The total number of occupied intervals $N(L)$, that is, those in which at least one raindrop has been observed, is then counted. If the data form a one-dimension fractal, then we must have

$$N(L) \propto L^{-\gamma}, \tag{23}$$

where $\gamma$ is defined as the fractal dimension of the process. When plotting $N(L)$ as a function of $\log(L)$, a straight line with slope $-\gamma$ is obtained. Of course, when $L \to T$, $N(L) \to 1$, and, asymptotically, one should have

$$\lim_{L \to T} N(L) = n = T/L.$$

Similarly, if $L$ is smaller than the minimum time separation between raindrops, $N(L) = m$, where $m$ is the total number of drops observed.

In any case, the behavior represented by (23) can occur only far from the two ends of the total observation period. Figure 9a shows the result of such an analysis when applied to the longest available period (4 months) of high-resolution data.

Except for the asymptotic regions mentioned above, the curve found (circles in Fig. 9a) is very close to a straight line with a slope, $-\gamma$, which has been found to be $-0.82$ and to prevail in the range from about $10^{-2}$ to $10^4$ min. When comparing these results to those found by Olsson et al. (1993), from which Fig. 9b was taken, a fundamental difference may be noted. Namely, in our case, a single fractal dimension is observed up to $10^4$ min, whereas the use of a 1-min time resolution tipping-bucket rain gauge leads to a three-segment curve with slopes of $-0.82$, $-0.37$, and $-1$ for increasing box lengths $L$. A first change in slope occurs near the 45-min abscissa.

The equality of the obtained fractal dimensions ($-0.82$) for smaller $L$ suggests that the second segment obtained by Olsson et al. may be an instrumental effect, as the integration inherent to the measurement principle of rain gauges has a strong influence on the obtained data. This point of view is corroborated by the influence of the threshold value on the fractal dimension (Olsson et al. 1993).

Assuming the Complete Bi-Pareto model provides an accurate representation of the temporal behavior of rain, it should then be possible to directly infer the curve in Fig. 9a from the model. Thus, let an arbitrary time in-

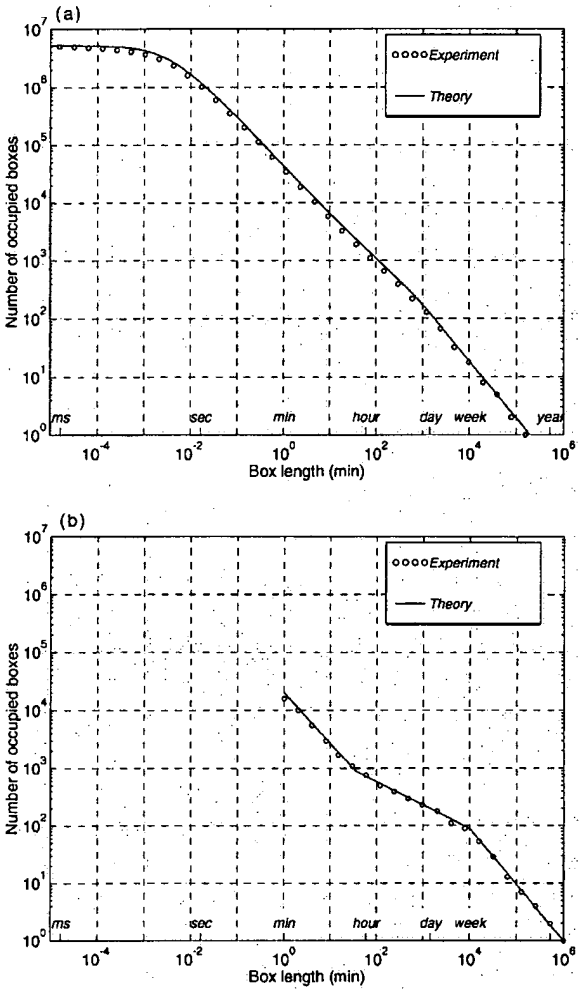


FIG. 9. (a) Box-counting distributions $N(L)$ for the 4-month data (O) and derived from the Complete Bi-Pareto model (———). (b) Experimental box-counting distribution $N(L)$ for 2-yr measurements (O) with best fit (———) from Olsson et al. (1993).

terval be of length $L$. Then the probability that it is "occupied" is equal to the probability that at least one drop falls into this interval, or, in other words, is the value of the cumulative distribution function of the residual lifetime taken at time $L$. Using the cumulative distribution (6), this leads to

$$G(L) = \int_0^L \frac{1 - F(\tau)}{\mu} d\tau = \int_0^L \frac{e^{-\lambda_0 \tau}}{\mu} \left[ \frac{pa^\alpha}{(\tau + a)^\alpha} + \frac{qb^\beta}{(\tau + b)^\beta} \right] d\tau.$$

If the total observation time $T$ is divided into $n$ intervals of length $L$, the theory of large numbers may be applied for estimating the mean value of the occupied intervals:

$$\langle N(L) \rangle = \frac{T}{L} G(L),$$

or

$$\langle N(L) \rangle = \frac{T}{\mu L} \int_0^L e^{-\lambda_0 \tau} \left[ \frac{pa^\alpha}{(\tau + a)^\alpha} + \frac{qb^\beta}{(\tau + b)^\beta} \right] d\tau. \quad (24)$$

Expression (24) is either evaluated by means of incomplete gamma functions or directly through a simple quadrature. The result obtained based on the parameters (2) found for the Complete Bi-Pareto model is plotted in Fig. 9a (solid curve).

A very good agreement can be noticed between the theoretical and experimental curves except for a slight vertical offset. This offset is likely due to an insufficiently accurate estimation of the average interdrop interval $\mu$, which in turn is derived from parameter $\lambda_0$ that has been shown to be known only approximately. This result corroborates the assumption of independence of raindrop times of arrival and therefore strengthens the validity of our modeling in terms of renewal processes.

It should also be underlined that the proposed model is richer than the fractal approach alone, which may also be suspected to be very sensitive to thresholding.

## 6. Conclusions

The use of a high-resolution disdrometer allowed a raindrop time-of-arrival time series to be obtained in combination with their sizes. An analysis of this time series over a total duration of 14 months, with a maximum of 4 continuous months, led to the following conclusions.

- The time series can be interpreted as the result of a renewal process whose survival law is of the Complete Bi-Pareto type.
- The survival law is related to the size distribution.

The interest of the model, in addition to a very good agreement with the collected data, also resides in its ability to explain various aspects (e.g., precipitation intensity and fractal behavior) of rain.

Two applications useful in the fields of meteorology and telecommunications have been shown and provide a good validation of the model.

Some particular aspects however still deserve attention.

- The influence of small raindrops currently incorrectly measured down to a minimum diameter of 0.3 mm. Although such an accuracy may at first seem to be an achievement for this kind of apparatus, the measured distribution curves and derived models show that measuring even smaller diameters should be made possible.
- The model's universality. Can rain be described by

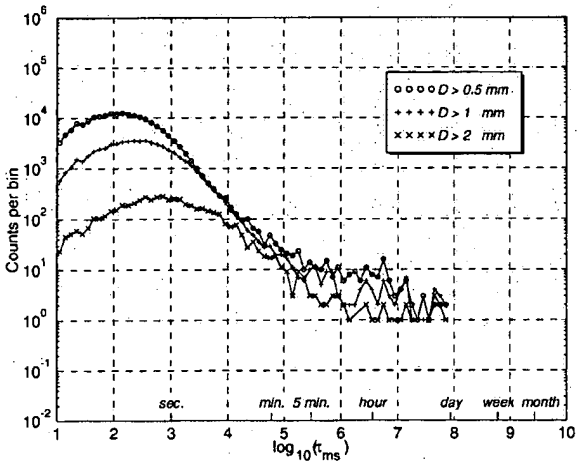


FIG. 10. Effect of diameter selection threshold on interdrop time distribution (3-week period).

means of the same model anywhere in the world? Of course, nothing allows such a conclusion to be drawn. However, the fact that the same fractal dimension is found in Paris and Sweden is encouraging.

Other more fundamental aspects, such as the combination of spatial and temporal effects, were not analyzed here and would allow further applications of the model to be envisioned in various fields, such as telecommunications, etc.

Nevertheless, the suggested model seems to be of sufficient interest that further experiments, it is hoped, may be carried out in other climatic conditions and over longer uninterrupted time periods in order to find different values for its climate-dependent parameters.

*Acknowledgments.* This research was supported by France Telecom's Centre National d'Etudes des Télécommunications at Belfort (CNET/BEL/POH). We are very grateful to D. Creutin from LETHE in Grenoble for providing us with the acquisition software allowing measurements of individual drop times of arrival, diameters, and velocities. Our thanks also go to Philippe Waldteufel for the interest he showed in this study and the useful advice he has provided us.

## APPENDIX A

### Effect of a Diameter Threshold for Selecting Analyzed Data

In section 4a we showed how to derive a joint representation of experimental distributions of interarrival times and drop sizes. The only remaining "free" parameter was $D_1$. For the time being, it may not be derived, as it is apparently related to the disdrometer's sensitivity level. In addition, parameter $\lambda_0$ was estimated only from long-term data that covered a much longer and therefore different time period than those that led to $a$, $b$, $\alpha$, $\beta$, and $q$. Therefore, its value should be considered only as an indication. Nevertheless, this model appropriately describes observations and this, over long durations, was far from obvious at first sight.

However, it may be wondered whether rejecting raindrops with sizes less than 0.3 mm from interdrop interval data as well as from drop diameter data, as was done here, had any effect on the model's shape. The model itself provides an answer to this question, as one of its key properties is a mixture between a size (or velocity) distribution and an exponential survival law. Accordingly, the renewal process can be divided into subprocesses corresponding to different drop size classes. A classical computation (e.g., Feller 1957) shows that if drops are selected with sizes that, for example, lie within a range $I = [D_{\min}, D_{\max}]$, a new regenerative process is generated, the distribution function of which has the following Laplace transform over an interval $I$:

$$f_I(s) = \frac{f(s)u}{1 + (u - 1)f(s)},$$

where $u = \text{Prob}[D_{\min} < D < D_{\max}]$.

For times ranging from a few minutes to a few hours, $f(s)$ can be read as $f(s) \approx 1 - g(s)$ with $g(s) \ll 1$ and $g(s)_{s\to 0} \to 0$. Under the same conditions, the following result may be obtained:

$$f_I(s) \approx 1 - \frac{g(s)}{u}.$$

Since the shape of $f(\tau)$, for $\tau \to \infty$, is directly related to that of its Laplace transform, for $s \to 0$, it may be expected that the slope of $f_I(\tau)$, in logarithmic coordinates, for large $\tau$'s, remains unchanged whatever the chosen $I$ interval. Figure 10, which gives the histograms corresponding to four drop size selection thresholds [$D > 0.5$ mm (○), $D > 1$ mm (+) and $D > 2$ mm (×)], is in very good agreement with this conclusion except for the fluctuations in the tail portion of the distributions, which are due to the reduced number of drops after selection.

It therefore appears that the model was not changed by eliminating drops smaller than 0.3 mm from the dataset.

## APPENDIX B

### Computation of the Precipitated Water Height

Let us consider the time interval $T_n$ between $n$ raindrops and determine its distribution, with an arbitrary time origin:

$$T_n = \tau_r + \sum_{i=1}^{n-1} \tau_i. \qquad \text{(B1)}$$

The $\tau_i$'s are independent, identically distributed random variables with a probability distribution $f(\tau)$ given

by (7). The variable $\tau_r$ is also independent of $\tau_i$ and is the residual survival time whose probability law is given by

$$f_1(\tau_r) = \frac{1 - F(\tau_r)}{\mu}. \quad \text{(B2)}$$

Thus, $T_n$ follows a probability density function that is obtained through multiple convolution, namely,

$$k_n(t) = f_1 * f^{(n-1)(*)} \quad \text{(B3)}$$

Taking its Laplace transform (keeping the same notations for functions and their Laplace transforms), where $s$ is the variable in the Laplace space, and using obvious notations leads to

$$k_n(s) = f_1(s)f(s)^{n-1} = \frac{1 - f(s)}{\mu s} f(s)^{n-1}. \quad \text{(B4)}$$

If $R(t)$ is the number of drops fallen during interval $[0, t]$, the probability that it is less than $n$ is

$$\Pr\{R(t) \leq n\} = \Pr(T_n > t) = 1 - K_n(t), \quad \text{(B5)}$$

where $K_n$ is the cumulative distribution function corresponding to density function (B3): namely,

$$K_n(t) = \int_0^t k_n(x)\, dx$$

and, of course, $K_0(t) = 1$. From (B5), the probability $\Pi_n(t)$ that $R(t) = n$ can be defined as

$$\begin{aligned} \Pi_n(t) &= \Pr\{R(t) = n\} \\ &= \Pr\{R(t) \geq n\} - \Pr\{R(t) \geq n - 1\} \\ &= K_n(t) - K_{n-1}(t), \end{aligned} \quad \text{(B6)}$$

where $R(t)$ is an integer random variable with a generator function $g(z, t)$ given by

$$g(z, t) = \sum_{n=0}^{\infty} \Pi(t) z^n. \quad \text{(B7)}$$

Laplace transforming (B7) over variable $t$ leads to

$$g(z, s) = \sum_{n=0}^{\infty} \Pi(s) z^n.$$

Since $K_n(s) = k_n(s)/s$ and $K_0(s) = 1/s$,

$$g(z, s) = \frac{1}{s} + \frac{f_1(s)}{s}\left[\sum_{n=0}^{\infty} (f^{n-1} - f^n) z^n - 1\right],$$

which, after summation of the geometrical series, leads to

$$g(z, s) = \frac{1}{s} + \frac{f_1(s)}{s} \frac{1 - z}{1 - z f(s)}. \quad \text{(B8)}$$

Besides, a raindrop of diameter $D$ and volume $v = \pi D^3/6$, falling through a collecting surface area $A$, contributes a water height $h = v/A = \pi D^3/6A$. The probability density function of $h$ is derived from that of $D$ since

$$p(h) = p(D)\left|\frac{dD}{dh}\right|.$$

Its Laplace transform is directly obtained as

$$p(u) = \int_0^{\infty} p(h) e^{-hu}\, dh \int_0^{\infty} e^{-(u\pi D^3/6A)} p(D)\, dD. \quad \text{(B9)}$$

Actually, the total water height $H(t)$, fallen over interval $[0, t]$, is a cumulative process since in our model the drop sizes are independent of arrival times. Using the total probabilities theorem, the probability density function of $H$ can then be written

$$\begin{aligned} q(h, t) &= \Pr\{h < H \leq h + dh\} \\ &= \sum_{n=0}^{\infty} \Pi_n(t) \Pr\{h < H \leq h + dh|_{R(t)=n}\}. \end{aligned}$$

Applying a Laplace transform over variable $h$ gives

$$q(u, t) = \sum_{n=0}^{\infty} \Pi_n(t) p^n(u). \quad \text{(B10)}$$

A comparison of (B10) and (B7) immediately shows that a second Laplace transform over variable $t$ gives $q(u, s) = g[p(u), s]$ or, explicitly,

$$q(u, s) = \frac{1}{s} + \frac{f_1(s)}{s} \frac{1 - p(u)}{1 - p(u) f(s)}. \quad \text{(B11)}$$

A dual Laplace transform of the cumulative distribution function can then be written as

$$Q(u, s) = \frac{1}{su} + \frac{f_1(s)}{su} \frac{1 - p(u)}{1 - p(u) f(s)}.$$

The complementary distribution $Q_c(h, t) = \Pr\{H > h, t\}$ has a dual Laplace transform of the form

$$Q_c(u, s) = \frac{1 - f(s)}{\mu u s^2} \frac{1 - p(u)}{1 - p(u) f(s)}. \quad \text{(B12)}$$

Theoretically, the problem is "solved." Unfortunately, it was not possible to find an analytical inversion for (B12).

## APPENDIX C

### Variability of the Precipitated Water Height

Let $N$ be the number of drops counted over interval $[0, t]$. Each drop $i$ contributes a water height $h_i$, which is independent and identically distributed with a distribution $p(h)$. The total water height fallen during the same time interval is given by

$$H = \sum_{i=1}^{N} h_i. \quad \text{(C1)}$$

Thus, $H$ appears to be a random sum of independent and identically distributed random variables. A conven-

tional computation (e.g., using Laplace transforms) gives the average value, which is nothing but (16), and the variance $\sigma_H^2 = [\langle N^2\rangle - \langle N\rangle^2]\langle h\rangle^2 + [\langle h^2\rangle - \langle h\rangle^2]\langle N\rangle$, or

$$\sigma_H^2 = \sigma_N^2\langle h\rangle^2 + \sigma_h^2\langle N\rangle. \tag{C2}$$

Here, $\langle h\rangle^2$ and $\sigma_h^2$ can be computed easily from the drop size distribution, and $\langle N\rangle = t/\mu$ and $\sigma_N$ can be appropriately approximated by using (Karlin and Taylor 1975) $\sigma_N^2 \approx t\sigma^2/\mu^3$, where $\sigma^2$ is the survival law's standard deviation. A computation involving a Laplace transform shows that for our model

$$\langle \tau^2\rangle \approx 2p\frac{a}{\lambda_0} + 2qb^\beta(1-\beta)\lambda_0^{\beta-2} \tag{C3}$$

or, with the numerical values found, $\langle \tau^2\rangle = 6.1 \times 10^{10}$. Thus, $\sigma = 2.5 \times 10^5$, the second term of (C2), is negligibly small relative to the first one, and the standard deviation of $H$ may be written

$$\sigma_H \approx \langle H\rangle\left(\frac{\sigma^2}{t\mu}\right)^{1/2}. \tag{C4}$$

During a year, (C4) leads to $\sigma_H/\langle H\rangle \approx 3\%$, and during a period of 1 month to

$$\frac{\sigma_H}{\langle H\rangle} \approx 11\%.$$

## REFERENCES


Atlas, D., and C. Ulbrich, 1977: Path- and area-integrated rainfall measurements by microwave attenuation in the 1–3-cm band. *J. Appl. Meteor.*, **16,** 1322–1331.

Best, A. C., 1950: The size distribution of raindrops. *Quart. J. Roy. Meteor. Soc.*, **76,** 16–36.

Feingold, G., and Z. Levin, 1986: The lognormal fit to raindrop spectra from frontal convective clouds in Israel. *J. Appl. Meteor.*, **25,** 1346–1363.

Feller, W., 1957: *An Introduction to Probability Theory and Its Applications.* 2d ed. Wiley and Sons, 354 pp.

Gloaguen, C., and J. Lavergnat, 1995: Raindrop size distribution near Paris. *Electron. Lett.*, **31** (5), 405–406.

Harris, C. M., 1968: The Pareto distribution as a queue service discipline. *Operations Res.*, **16,** 307–313.

Hauser D., P. Amayenc, B. Nutten, and P. Waldteufel, 1984: A new optical instrument for simultaneous measurements of raindrop diameter and fall speed distribution. *J. Atmos. Oceanic Technol.*, **1,** 256–269.

Hosking, J. G., and C. D. Stow, 1988: The arrival rate of raindrops at the ground. *J. Climate Appl. Meteor.*, **26,** 433–442.

Hughes, C. D., 1993: The Olympus utilization programme. *Olympus Utilization Conf.*, Sevilla, Spain, European Space Agency. [Available from ESA-ESTEC TOS-EEP, Keplerlaan 1, PB 299, NL-2200 AG, Noordwijk, the Netherlands.]

ITU-R, 1990: Attenuation by hydrometeors, in particular precipitation, and other atmospheric particles. International Telecommunications Union Rep. 721-3, 226–245.

Karlin, S., and H. M. Taylor, 1975: *A First Course in Stochastic Processes.* Academic Press, 557 pp.

Lavergnat, J., and CNET Work Group, 1988: The French propagation experiment with Olympus. *Proc. 11th Meeting of Olympus Propagation Experimenters,* Copenhagen, Denmark, European Space Agency, 37–56. [Available from ESA-ESTEC TOS-EEP, Keplerlaan 1, PB 299, NL-2200 AG, Noordwijk, the Netherlands.]

Laws, J. O., and D. A. Parsons, 1943: The relation of raindrop size to intensity. *Trans. Amer. Geophys. Union,* **24,** 452–460.

Lovejoy, S., and B. Mandelbrot, 1985: Fractal properties of rain and a fractal model. *Tellus,* **37A,** 209–232.

Marshall, J. S., and W. McK. Palmer, 1948: The distribution of raindrops with size. *J. Meteor.*, **5,** 165–166.

Olsson J., J. Niermczynowicz, and R. Berndtsson, 1993: Fractal analysis of high-resolution rainfall time series. *J. Geophys. Res.*, **98** (D12), 23 265–23 274.

Segal, B., 1986: The influence of rain gage integration time on measured rainfall intensity distribution functions. *J. Atmos. Oceanic Technol.*, **3,** 662–671.

Smith, J. A., 1993: Marked point process models of raindrop-size distributions. *J. Appl. Meteor.*, **32,** 284–296.

——, and A. K. Karr, 1983: A point process model of summer season rainfall occurrences. *Water Resour. Res.*, **19,** 95–103.

Srivstava, R. C., 1971: Size distribution of raindrops generated by their breakup and coalescence. *J. Atmos. Sci.*, **28,** 410–415.

Waymire, E., and V. K. Gupta, 1981: The mathematical structure of rainfall representations *Water Resour. Res.*, **17,** 1261–1294.